AIAA 98-3713

Summary of Inlet Characteristics of the F/A-18A High Alpha Research Vehicle

Kevin Walsh
NASA Dryden Flight Research Center
Edwards, California

William Steenken and John Williams
General Electric Aircraft Engines
Evendale, Ohio

34th AIAA/ASME/SAE/ASEE
Joint Propulsion Conference and Exhibit
July 13–15, 1998 / Cleveland, OH

SUMMARY OF INLET CHARACTERISTICS OF THE F/A-18A HIGH ALPHA RESEARCH VEHICLE

Kevin Walsh*
NASA Dryden Flight Research Center
Edwards, California

William Steenken† and John Williams‡
General Electric Aircraft Engines
Evendale, Ohio

Abstract

Effects of high-angle-of-attack flight on aircraft inlet aerodynamic characteristics were investigated at NASA Dryden Flight Research Center as part of NASA's High Alpha Technology Program. The highly instrumented F/A-18A High Alpha Research Vehicle was used for this research. A newly designed inlet total-pressure rake was installed in front of the right-hand F404-GE-400 engine to measure inlet recovery and distortion characteristics. Objectives included (1) determining the inlet total-pressure characteristics at steady high-angle-of-attack conditions, (2) assessing if inlet distortion is significantly different between rapid angle-of-attack maneuvers and corresponding steady aerodynamic conditions, (3) assessing inlet characteristics during aircraft departures, (4) providing data for developing and verifying computational fluid dynamic codes, and (5) calculating engine airflow using four methods for comparison with a reference method. This paper describes the results obtained from this investigation. These data and the associated database were rigorously validated to establish the foundation for understanding inlet characteristics at high angle of attack.

Nomenclature

AIP	aerodynamic interface plane
ALF	aft looking forward
AOA	angle of attack, deg
AOSS	angle of sideslip, deg
CFD	computational fluid dynamics
CROCP	combined rate of change of aircraft motion, deg/sec
CVG	compressor vane guide position, deg
D2	simple distortion intensity descriptor, e.g. $(PT_{max} - PT_{min})/PT_{avg}$
DFRC	Dryden Flight Research Center, Edwards, California
DP/PC	circumferential distortion descriptor
DP/PR	radial distortion descriptor
DPRS	predicted loss of stability pressure ratio
DPRSF	predicted loss of stability pressure ratio for the fan
DPRSH	predicted loss of stability pressure ratio for the compressor
FS	fuselage station
GEAE	General Electric Aircraft Engines, Evendale, Ohio
HARV	High Alpha Research Vehicle
HATP	High Alpha Technology Program
IGV	inlet guide vane
INS	inertial navigation system
L/D_{ENG}	length per unit diameter of the engine
LEX	leading-edge extension
MDA	The Boeing Company (formerly McDonnell Douglas Corporation, St. Louis, Missouri)
PCM	pulse code modulation
PSE	low-response inlet static pressure, psid
PSK	high-response static pressure, psia
PT	total pressure, psia

*Aerospace Engineer.
†Aerospace Engineer.
‡Aerospace Engineer.

PT_{avg}	average AIP total pressure, psia
PT_{max}	maximum AIP total pressure, psia
PT_{min}	minimum AIP total pressure, psia
PTE	low-response total pressure, psid
PTK	high-response total pressure, psia
PT0	free-stream total pressure, psia
PT2	fan inlet total pressure, psia
sps	samples/sec

Introduction

Inlet pressure distortion affects on a propulsion system at high angle of attack (AOA) during steady aerodynamic conditions, rapid aircraft maneuvers, and aircraft departures are not thoroughly understood. A team of NASA and industry researchers was formed as part of the NASA High Alpha Technology Program (HATP) to investigate the inlet characteristics, inlet and engine compatibility, and prediction methodologies at high-AOA conditions. This effort addressed questions that have arisen during past subsonic aircraft development programs. These questions included the following subjects:

- How do the inlet total-pressure characteristics, such as inlet recovery, circumferential and radial distortion, planar wave, and turbulence, behave as a function of AOA, angle of sideslip (AOSS) and Mach number?
- How do inlet distortion levels during rapid, high-AOA maneuvers compare with distortion levels at corresponding steady aerodynamic flight conditions?
- What are the characteristics of the inlet flow during aircraft departures? What factors lead to engine stalls that have been experienced during aircraft departures? Are there any other significant factors beyond inlet-induced distortion which account for engine stalls?
- Can computational fluid dynamics (CFD) technology be used to accurately predict inlet characteristics at high-AOA conditions?
- Are the engine airflow pumping characteristics affected at extreme aircraft maneuver conditions? What is the best method for measuring airflow in flight at these conditions?

To address each of these questions, flights to map inlet characteristics as a function of AOA, AOSS, and Mach number were conducted using the F/A-18A High Alpha Research Vehicle (HARV). Inlet data obtained at steady aerodynamic conditions formed the foundation for this inlet research effort.

The HARV aircraft, flown at the NASA Dryden Flight Research Center (DFRC), Edwards, California, provided the ideal platform for the controlled exploration of inlet characteristics related to highly agile full-scale vehicles.[1] The thrust-vectoring vane system provided the ability to maintain steady, high-AOA conditions. The aircraft was highly instrumented with emphasis on the region around, and in, the starboard inlet and engine. A newly developed, 40-probe, total-pressure, inlet rake was installed directly ahead of the engine.[2] Surface static-pressure transducers were installed at the inlet rake location and around the inlet lip. High-frequency response instrumentation was installed to monitor engine operation and behavior. To maintain the quality of the high-response data, a series of specific instrumentation calibrations was performed on the ground and in flight during the test program.

This paper summarizes the inlet total pressure data, such as recovery, turbulence, and distortion obtained during the HARV inlet program. Data are presented for the specific aircraft maneuvers flown, such as steady aerodynamic conditions,[3] rapid changes in AOA and AOSS,[4] and aircraft departures.[5] The HARV flight test data were also used to evaluate and improve a CFD approach for predicting dynamic distortion[6] and to estimate engine airflow with clean and distorted airflows.[7]

Use of trade names or names of manufacturers in this document does not constitute an official endorsement of such products or manufacturers, either expressed or implied, by the National Aeronautics and Space Administration.

HARV Inlet Program Objectives

The HARV inlet program objectives were developed from questions raised from previous inlet research programs. To understand these objectives, a historical perspective of the traditional methods for obtaining inlet distortion and its subsequent influence on inlet–engine compatibility is presented. Then, a brief summary of each part of the inlet research program is provided.

Historical Perspective

In developing an air-breathing propulsion system, designers seek a high degree of aerodynamic compatibility between the inlet and engine. This

compatibility is especially true for high-performance combat aircraft with high-AOA-maneuvering requirements. The current state-of-the-art process to achieve inlet–engine compatibility involves several extensive inlet and engine test programs and close interaction between the airframe and engine companies. These tests separately determine inlet distortion generation and engine distortion tolerance characteristics. Understanding inlet distortion levels is needed at the earliest possible stage of the design process to perform trade studies.

Inlet–engine compatibility is established by determining the worst-case level of inlet total-pressure distortion to which an engine will be subjected. The impact of this distortion on the aerodynamic stability of the engine is then assessed. In general, this assessment is accomplished by testing inlet-forebody scaled models in a wind tunnel at fixed attitudes covering a range of inlet airflows, Mach numbers, AOA, and AOSS that are projected to be encountered by the aircraft during its service life. The resulting time-variant, total-pressure, distortion patterns that cause the maximum loss in compression component stability margins are then determined. Compression components are designed to have sufficient stability margin to cover both the external destabilizing influence of total-pressure distortion determined from the wind-tunnel data and the internal destabilizing influences, such as engine variability, deterioration, control tolerances, and throttle transients. This technique successfully provides compatible inlet–engine systems on many commercial and military propulsion systems.

Inlet compatibility engineers have long been concerned that the maximum total-pressure distortion levels determined during fixed-attitude testing in wind tunnels may not represent the maximum total-pressure distortion levels encountered during maneuvering flight. Two fundamental concerns existed. First, is the maximum level of distortion obtained from fixed-attitude testing adequate for predicting the maximum total-pressure distortion obtained at similar aerodynamic conditions during maneuvering flight? Second, is it possible that unsteady flow disturbances associated with the fuselage forebody, protuberances, or both, would be missed between fixed-attitude test points? The HARV inlet research program was designed to provide the information that would help answer these questions by obtaining full-scale flight data at steady aerodynamic conditions and during maneuvering flight at comparable conditions.

Inlet Distortion at Steady Aerodynamic Conditions

The inlet data obtained at steady aerodynamic conditions provided the foundation for comparing and analyzing inlet characteristic data during rapid AOA maneuvers, aircraft departures, and CFD predictions. The objective was to document inlet characteristics at Mach 0.3 and Mach 0.4 and at various stabilized AOA and AOSS conditions.

Inlet Distortion During Rapid AOA Maneuvers

Rapid AOA maneuvers were conducted to determine whether results obtained for steady aerodynamic conditions were adequate for describing the inlet-generated, total-pressure distortion levels which occur during such maneuvers. The evaluation focused on whether the constrained steady aerodynamic condition test matrix describes inlet trends in sufficient detail as currently practiced. If the results of the rapid AOA maneuvers at any condition showed a significant increase in peak level distortion when compared with the steady aerodynamic condition results, the inlet data would be analyzed to determine the source of these increased peak distortion levels. The affects of rapid AOA maneuvers on inlet distortion levels can best be assessed during flight tests.

Inlet Distortion During Aircraft Departures

An aircraft departure, or departed flight, occurs when an aircraft is flown in regimes where the control surfaces no longer have sufficient effectiveness to fully control the flightpath of the aircraft. The aircraft enters a series of self-induced motions that represent a departure from normal aircraft trajectories. In general, this type of flight is only encountered by military pilots who push their aircraft to extreme AOA and AOSS. However, inlet compatibility engineers have long been interested in knowing the manner in which the aircraft inlet flow behaves during departures. If engine stalls should occur during a departure, engineers want to know the parameters that contributed to the stall.

For these reasons, a series of aircraft departures were conducted to try to induce engine stalls. The objectives were to quantify the performance of the inlet during a departure in terms of inlet recovery and dynamic distortion characteristics and to gain insight into the causes of engine stalls.

Dynamic Distortion Prediction Using a Combined CFD and Distortion Synthesis Approach

Computational fluid dynamics has been under continuous and wide-spread development since the late

1960's. The CDF offers distinct advantages that can be performed at any stage of the airframe development process. Methods were developed during the 1970's and 1980's to improve the ability to predict inlet performance. These methods, known as distortion synthesis, use a random number process to synthesize the fluctuating component of the instantaneous total pressure from the statistical properties of the inlet pressure data.[8]

Turbulence modeling remains one of the most significant challenges in CFD. Notable advancements have been made over the past several years, including many formulations of two-equation models. A sufficiently accurate CFD solution, using a two-equation turbulence model, can be used to obtain the required inputs for a distortion synthesis procedure. This procedure would permit predicting peak dynamic distortion before costly wind-tunnel or flight tests.

A procedure was developed and evaluated by The Boeing Company (formerly McDonnell Douglas Aircraft (MDA) Corporation, St. Louis, Missouri) using flight data obtained from the HARV. This procedure involved a combined approach of (1) obtaining a CFD steady-state prediction of the inlet diffuser flowfield, (2) obtaining the correlation of the computed data with root-mean-squared (RMS) turbulence, and (3) generating estimates of the peak dynamic distortion using a synthesis approach. Reference 6 describes the procedure in detail.

Estimating Engine Airflow with Clean and Distorted Airflow

Engine airflow is an important parameter when addressing turbofan engine-powered aircraft issues. For example, inlet distortion is often correlated with engine airflow corrected to the aerodynamic interface plane (AIP). The AIP engine airflow is also an important part of the net thrust calculation.

The HARV provided a unique opportunity to address the difficult issue of providing reliable estimates of in-flight-determined, total-engine airflow. The objective was to compare three methods of correlating and estimating airflow with one method having three variants. Reference 7 describes the methods for obtaining in-flight airflow. Ground-test-cell flow calibration of the engine and establishment of flow correlations for each method in flight at minimum inlet flow distortion conditions were crucial to the success of evaluating the airflow methods.

Airplane Description

Figure 1 shows the HARV, a single-place F/A-18A aircraft (pre-production aircraft number 6) built by MDA and the Northrop-Grumman Corporation (Newbury Park, California). The F/A-18A HARV is powered by two modified F404-GE-400 turbofan engines (General Electric Aircraft Engines (GEAE), Evendale, Ohio). Wing leading-edge extensions (LEX) are located on each side of the fuselage from the wing roots to just forward of the windshield. This aircraft was modified with extensive instrumentation and multiaxis thrust-vectoring paddles. Thrust vectoring provided the HARV with the ability to fly at sustained, aerodynamic attitudes beyond the capabilities of conventional high-performance aircraft.

EC91 495-15

Figure 1. NASA F/A-18A HARV aircraft (preproduction aircraft number 6) with multiaxis thrust-vectoring paddles.

Propulsion System Description

The F/A-18A aircraft inlets are fixed-geometry, external compression inlets with 5° compression ramps mounted on the sides of the aircraft fuselage. Inlets are located approximately 25 ft aft of the aircraft nose under the LEX of the wing (fig. 1). Figure 2 shows a schematic of the air induction system, including key inlet dimensions. These inlets are located approximately 5 in. from the sides of the fuselage to avoid ingestion of the fuselage boundary layer. The subsonic diffuser makes a gradual transition from the inlet throat to the engine face which is centered approximately 12 in., or 0.4 duct diameter, above and 12 in. inboard of the inlet centroid. The diffuser is approximately 12 ft long with a resulting length per diameter of the engine (L/D_{ENG}) of

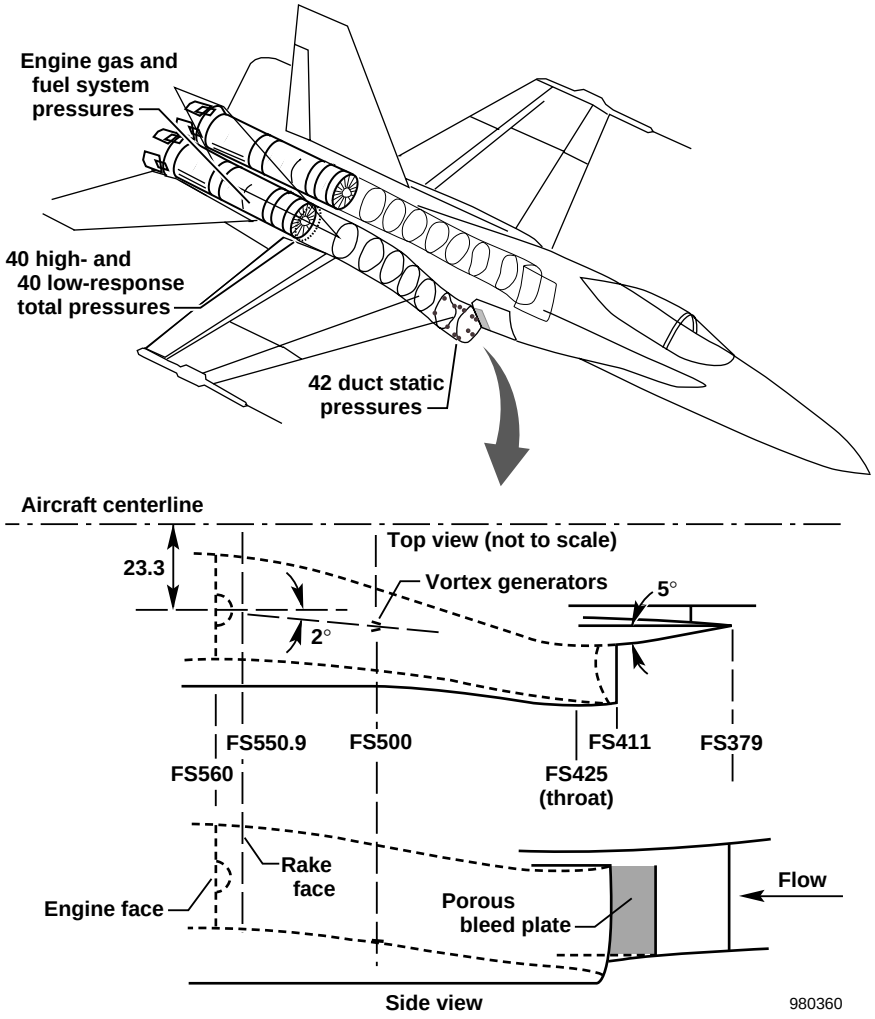

Figure 2. F/A-18A air induction system.

approximately 5.3. A pair of vortex generators is located on the lower surface of the diffuser to prevent local flow separation in this area.

The external and internal geometry of the inlet cowl lip was optimized for maneuvering in the subsonic, high-AOA region of the flight envelope. The lower and lower-inboard portions of the inlet lip were cut back and thickened to decrease the compressor face distortion at extreme aircraft attitudes. References 9, 10, and 11 provide further details of the F/A-18A air induction system.

Figure 3 shows the F404-GE-400 engine, a low bypass, twin-spool, and axial-flow turbofan with afterburner. Two single-stage turbines independently drive the three-stage fan and seven-stage high-pressure compressor. In the fan, the inlet-guide vanes (IGV) and the stators of the first stage are variable. In the high-pressure compressor, the IGV and the first two stator stages are variable. These variable IGV direct the inlet air at the optimum angle for efficient and stable engine operation. The through-flow annular combustor uses atomizing fuel nozzles, and the mixed-flow afterburner uses air from the bypass and from the high-pressure core. The F404-GE-400 engine control is an integrated system, using both hydromechanical and electronic control components. The uninstalled sea-level-static military thrust of each engine is approximately 10,700 lbf, and the maximum afterburner thrust is approximately 16,000 lbf. Maximum corrected airflow through the engine is approximately 144 lbm/sec.

Three thrust-vectoring vanes were mounted on the aircraft and positioned approximately 120° apart about the periphery of each engine behind the nozzle exits.

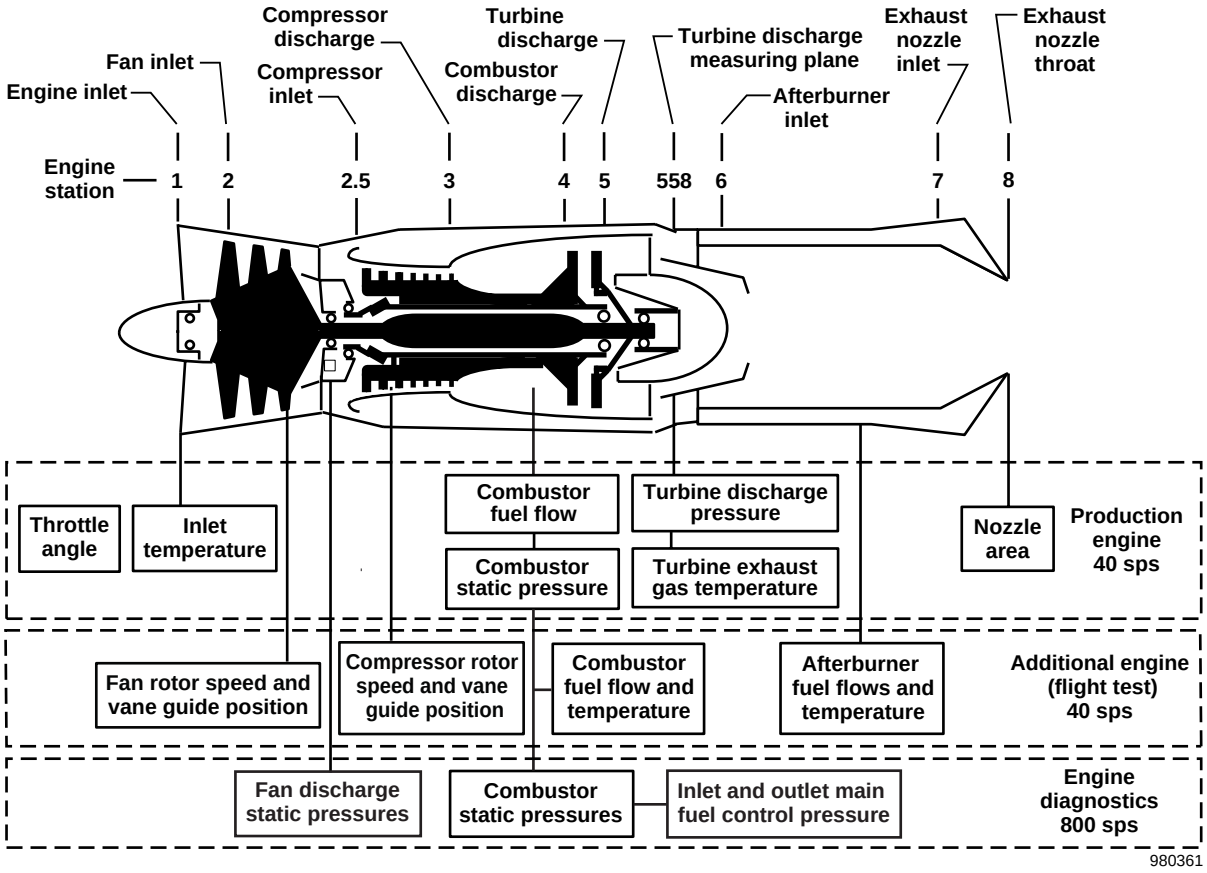

Figure 3. Right engine instrumentation supporting HARV inlet research program.

The corners of each vane were clipped to avoid interference with adjacent vanes at full deflection of 25°. These engines were modified to accommodate the thrust-vectoring vane installation by removing the divergent section of the nozzle. Reference 1 provides further details of the HARV thrust-vectoring vane system.

Instrumentation

The HARV inlet research objectives required accurate measurement of specific inlet, engine, and airdata parameters. These measurements were recorded during steady aerodynamic flight conditions up to 60° AOA, rapid AOA maneuvers, and aircraft departures with engine stalls.

Aircraft and Engine

Aircraft instrumentation included accelerometers, rate gyroscopes, surface position measurements, and airdata. A flight research airdata system consisting of swiveling pitot probes with conventional AOA and AOSS vanes was mounted on each wingtip. These probes swiveled freely for local AOA between –15° and 72° and for local AOSS between ±40°.[12]

Both engines had basic instrumentation for monitoring engine operation and were equipped with a real-time thrust measurement system.[13] Figure 3 shows the instrumentation that was added to the production engine instrumentation which included guide vane positions, fan and compressor speeds, fuel flows, and diagnostic pressures.

Inlet Rake

An innovative inlet total-pressure distortion measurement rake was developed for the F/A-18 A/B/C/D aircraft inlet by a team of NASA DFRC and GEAE personnel. The inlet rake was installed at the AIP, which is defined as the measurement plane between the inlet and engine. Inlet distortion and performance are determined in this measurement plane. For the F/A-18A, the AIP is located 4 in. in front of the bullet nose of the engine. The inlet rake consisted of a streamlined centerbody and eight aerodynamic rake legs. Each rake leg consisted of five dual probes located at the centroids

of five equal areas. The 40 dual probes measured high- and low-frequency response total pressures. Figure 4 shows the rake orientation and the nomenclature assigned to each pressure port. References 2, 3 and 14 describe the inlet rake. Orientation of the rake was similar to that used in previous F/A-18A inlet tests.[9]

The inlet rake probe was designed to be insensitive to airflow angularity, an important criterion when measuring total pressure in distorted flows. This configuration allowed the sensors to read true pressure levels of local airflow at yaw angles from ±25° and at pitch angles from 15° to –25° with positive angles being in the direction of the engine centerline. Blockage of total airflow at the AIP caused by the inlet rake probes was 0.4 percent, and the maximum blockage of the flow area caused by the rake structure was less than 8 percent. The rake structure was located 1.5 in. downstream of the AIP.

Inlet Low-Response Pressures

The low-frequency response static and total pressures (PSE and PTE) were measured using differential pressure transducers. To obtain the absolute pressures, an accurately measured reference pressure was added to the differential pressures. The right-hand aft looking forward (ALF) engine bay was selected as the reference pressure location.

Each differential transducer unit provided the measurement of 32 pressures. These units were thermally stabilized to minimize zero drift associated with temperature variations and were capable of in-flight calibrations.

Inlet High-Response Pressures

The high-frequency response static and total pressures (PSK and PTK) were measured using individual temperature-compensated pressure transducers. Each transducer was mounted at a rake measurement port in close proximity to a low-frequency response pressure probe. Calibration procedures for the high-frequency response transducers allowed accurate measurement of total and static pressures during rapid aircraft maneuvers and departures. The sample rate of these transducers was configured to 2143 samples/sec.

Inlet wall static pressure measurements at the inlet rake and around the inlet entrance were also obtained during the HARV inlet program. Results from these measurements are not included in this paper. Reference 3 provides further details of these total and static pressure instrumentation and calibration measurements.

Data Acquisition and Analysis

Data acquisition for the HARV inlet program used three pulse code modulation (PCM) systems. Two PCM systems telemetered aircraft and engine data to ground-based computers. The third recorded inlet specific data onboard the aircraft. To synchronize the three PCM

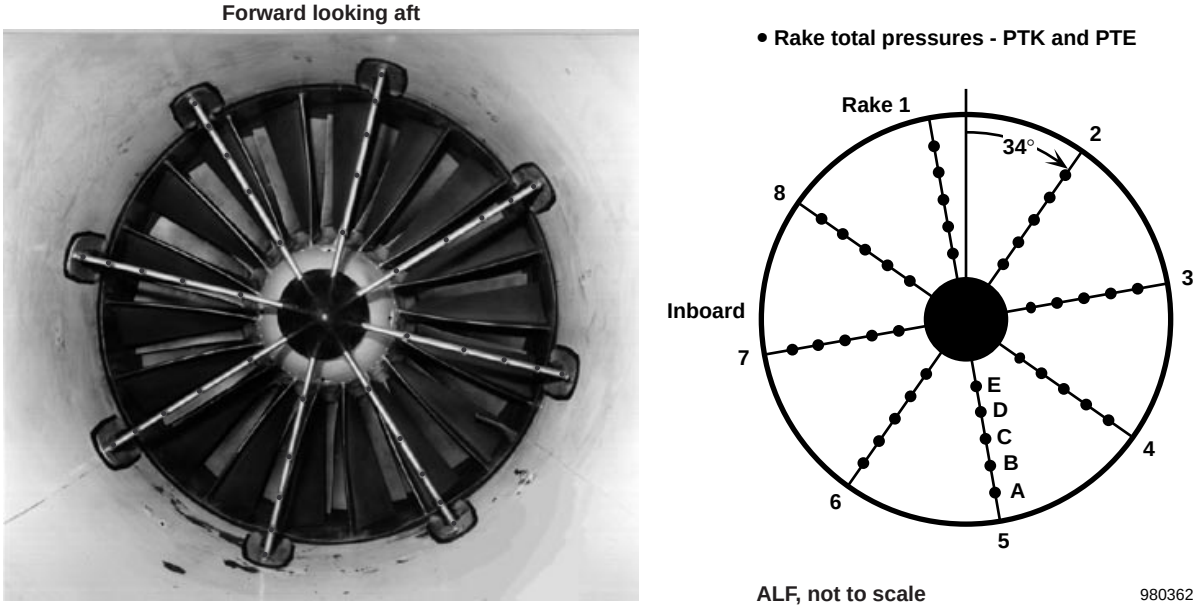

Figure 4. HARV inlet rake and instrumentation locations.

systems, an embedded time code was inserted into each data stream. These telemetered data were synchronized with the onboard recorded data to the fastest sample rate data which was 2143 samples/sec. Data obtained for each test condition were processed postflight, using data quality and analysis software to assure high-quality results.

Inlet Parameters

The analysis calculations included inlet characteristics, such as inlet recovery, circumferential and radial total-pressure distortion levels as well as planar wave and turbulence values. The software provided time-averaged and peak-pattern screening of the inlet characteristics. The inlet parameters were calculated based on industry standard guidelines[15, 16] and established GEAE methodology.[17, 18] Reference 3 provides additional details of the data acquisition and analysis methods.

Steady Aerodynamic Estimation Model

The inlet characteristics from the discrete steady aerodynamic conditions were transferred to data look-up tables to allow comparison with the time-variant conditions of the rapid aircraft maneuvers. These data tables and other inlet calculations for each inlet comparison parameter were estimated as a function of AOA, AOSS, and Mach number. A software application used these tables in combination with other inlet calculations to compute the comparison of the inlet parameters between steady aerodynamic estimations and the rapid aircraft maneuvers at equivalent AOA, AOSS, and Mach number conditions.

Trajectory Reconstruction

The AOA and AOSS vanes were calibrated to give accurate AOA and AOSS measurements during steady aerodynamic maneuvers. The calibration removes such aerodynamic affects on the indicated vane positions as local upwash, sidewash, and aircraft angular rates. These corrections are not valid during rapid aircraft maneuvers. In addition, AOA and AOSS measurement hysteresis during aircraft maneuvers make these measurements unreliable. An alternate source for the calculation of AOA and AOSS during aircraft maneuvers is the inertial navigation system (INS) onboard the aircraft. A procedure called trajectory reconstruction provides more accurate AOA and AOSS results than one using the data from the vanes. During aircraft maneuvers, INS, calibrated AOA and AOSS vanes, and winds aloft data are integrated. Trajectory reconstruction required 2 sec at steady aerodynamic conditions before a rapid aircraft maneuver.

Flight Test Description

A matrix of flight maneuvers was flown to evaluate the inlet research objectives. These maneuvers consisted of steady attitudes of AOA and AOSS, positive and negative sweeps of AOA, and aircraft departures. All testing was performed between military (maximum non-afterburning) and maximum afterburning power settings to maintain a constant corrected engine airflow of approximately 144 lb/sec. When at the required flight condition, the power setting was held steady while research data were recorded.

In-Flight Calibrations

During flight, calibrations of the inlet rake and duct, low- and high-response pressure transducers (PTE, PTK, PSE, and PSK) were performed just before a series of maneuvers. The calibration required constant altitude and airspeed for 15 sec. Reference 3 provides additional details of the calibration process.

Steady Aerodynamic Conditions

Seventy-nine flight maneuvers at steady aerodynamic conditions were conducted at Mach 0.3 and Mach 0.4 and from an altitude of 20,000 to 35,000 ft. Following pressure transducer calibration data collection, the length of recorded data for all maneuvers was established at 6 sec. However because of aircraft maneuver limitations, shorter data records were obtained at the extreme AOA and AOSS conditions. A successful maneuver required maintaining the flight condition tolerances. Tolerance for Mach number during all maneuvers was ±0.01. Tolerance for AOA and AOSS was ±1.0°. For the ±10° AOSS maneuvers, it was not possible for the airplane to maintain a 10° or –10° AOSS condition. As a result, the maximum sustainable AOSS condition was used. Reference 3 provides additional details of the steady aerodynamic flight conditions.

Rapid AOA Maneuvers

Forty-six aircraft maneuvers with rapidly changing AOA were performed by holding the initial Mach number, AOA, AOSS, and engine airflow for 2 to 3 sec. Table 1 shows the initial AOA and AOSS conditions.

After the steady conditions were held for 2 to 3 sec, a maximum rate AOA sweep was performed. Such sweeps were performed at negative and positive rates dependent on the initial AOA condition. The overall

maximum AOA rates achieved were –37 and 46 deg/sec. The end point of a maneuver was established when the Mach number exceeded 0.02 of the initial Mach number. Limiting the variation in Mach number ensured valid comparisons between the steady aerodynamic conditions and the rapid AOA maneuvers. The rapid AOA maneuver required a reversal in the AOA sweep once the pilot exceeded a maximum AOA limit (60° at Mach 0.3 and 40° at Mach 0.4) or minimum AOA limit (10° at both Mach 0.3 and Mach 0.4).

Table 1. Initial aerodynamic conditions for dynamic maneuvers.

Mach 0.3		Mach 0.4	
AOA, deg	AOSS, deg	AOA, deg	AOSS, deg
10	–5	10	–5
10	0	10	0
10	5	10	5
30	–5	13	–5
30	0	13	0
30	5	13	5
60	–2	40	–4
60	0	40	0-1
60	2-3	40	4

Aircraft Departures

Twelve high power departed flight maneuvers were performed between Mach 0.3 and Mach 0.4 at an entry condition of 35 kft. These high yaw rate departures were divided evenly between nose-left and nose-right maneuvers with increasing rates of change in yaw at entry. Throttles for both engines were set at military power at the start of the maneuvers and were reduced to idle power during the aircraft recovery phase.

Flight departure maneuvers were initiated by starting from a 1-*g* flight condition. The pilot increased AOA to between 50° and 60°. Then, either a left or right yaw rate was induced by moving the control stick to a position that produced the desired entry yaw rate. After the desired rate was achieved, the pilot initiated recovery of the aircraft from the departed flight condition by releasing the stick and allowing it to return to the neutral position. At the same time, the pilot moved the engine throttles to the idle power position. Reference 5 provides further details of departure flight maneuvers.

Engine Airflow Measurements

In-flight engine airflow measurements were obtained in two phases. First, inlet total pressure airflow data were obtained for 1-*g* level flight, at Mach 0.6, and at an altitude of 20,000 ft. These flight conditions correspond to minimum inlet airflow distortion levels. Second, airflow data were obtained during various steady aerodynamic conditions to evaluate airflow during low to high distortion levels and to determine what affect distortion has on the various airflow correlation methods.

Results and Discussion

This section summarizes the inlet rake data obtained during the HARV inlet program. Consistent results for 11 test points over the course of the flight test program were obtained at Mach 0.3, 30° AOA, and 0.0° AOSS.[3] Inlet performance data obtained at steady aerodynamic conditions show the affects of AOA, AOSS, and Mach number on inlet recovery, turbulence, and peak dynamic distortion. During rapid, high-AOA maneuvers, inlet distortion levels are compared with levels at corresponding steady aerodynamic flight conditions. Flight departure data are presented to show the cause of the engine stalls. A comparison of CFD inlet distortion prediction with flight data is then presented. Results from four airflow estimation methods are provided.

Inlet Performance at Mach 0.3

Figures 5 and 6 show the trends for inlet recovery, turbulence, and peak circumferential and radial distortion values as a function of AOA and AOSS at Mach 0.3. These data points represent time-averaged values. A solid symbol indicates that only one set of time-averaged data was obtained for the target AOA condition. The open symbols and the *x* indicate that multiple datasets were obtained at the target AOA condition. Positive AOSS indicate that the aircraft was pointing nose-left, windward for the right-hand inlet.

Inlet Recovery

Figure 5(a) shows the affect of AOA and AOSS on inlet pressure recovery. An inlet recovery value of 1.0 is the ideal value and indicates 100-percent pressure recovery at the AIP when referenced to the free-stream total pressure. Negative AOSS have an obvious detrimental affect on inlet recovery for all AOA,

showing the impact of flow washing over the fuselage. As AOA increases, the detrimental affect of AOSS becomes increasingly pronounced. Pressure recovery remains constant at approximately 97 percent for 4° to 30° AOA. As AOA increases above 30°, the loss in pressure recovery becomes increasingly sensitive to AOA. At 60° AOA and 0° AOSS, the pressure recovery has dropped below 91 percent.

Turbulence

Figure 5(b) shows the affect of AOA and AOSS on turbulence levels at Mach 0.3. The detrimental affects of

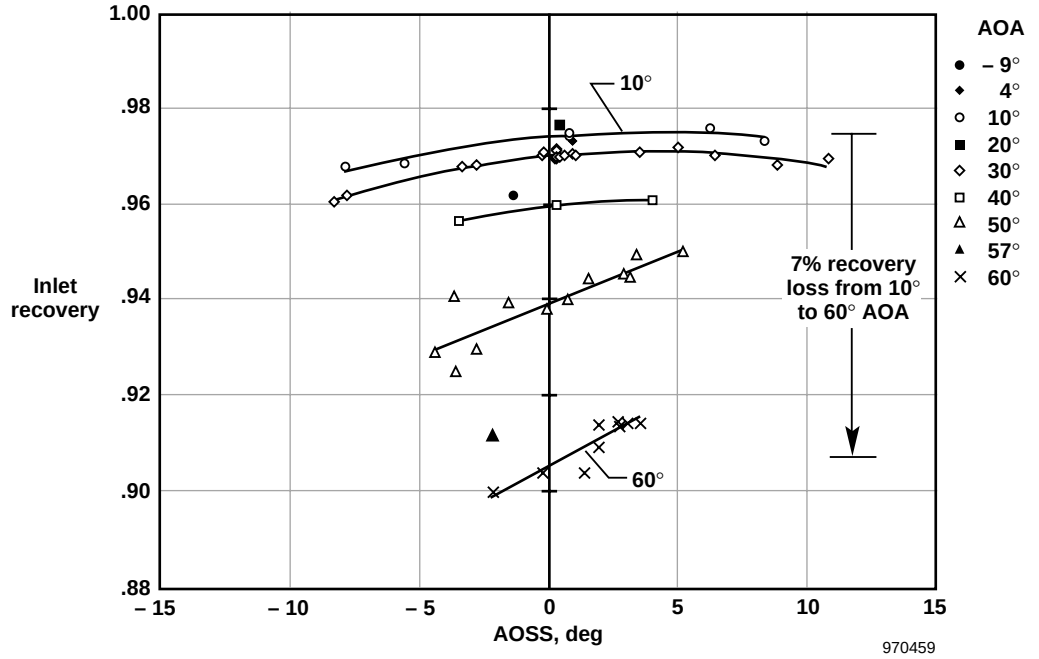

(a) Inlet recovery.

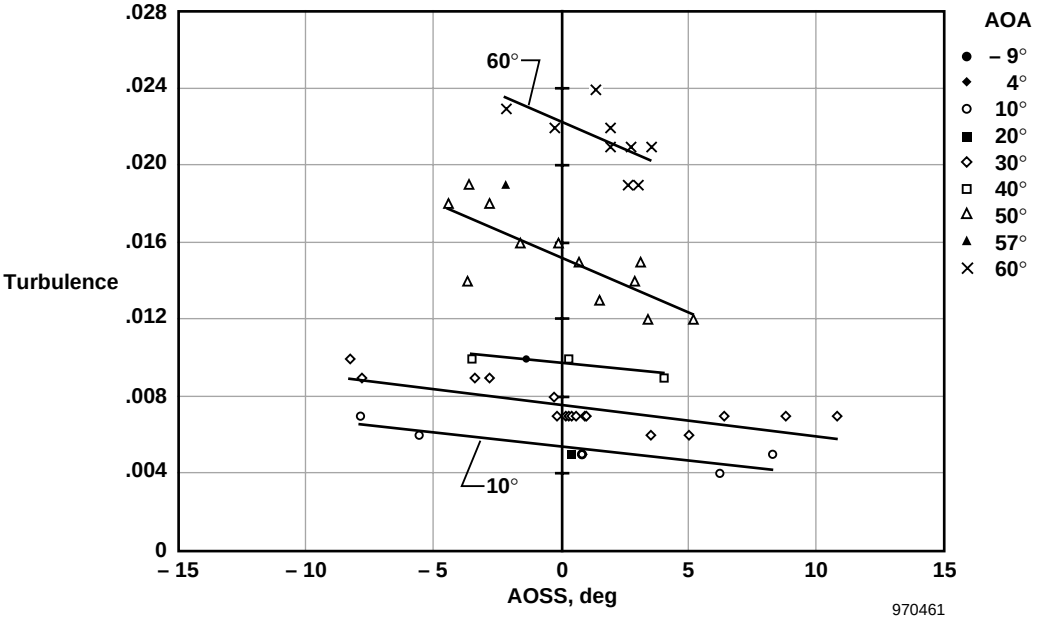

(b) Inlet turbulence.

Figure 5. Affect of AOA and AOSS on inlet recovery and turbulence during steady aerodynamic conditions at Mach 0.3.

AOA and AOSS on turbulence are similar to those shown for inlet recovery. Comparing figure 5(a) with figure 5(b) clearly shows that as the flow turbulence increases, inlet recovery decreases. Going from nose-left to nose-right (positive to negative AOSS) increases turbulence. From 4° to 20° AOA, the turbulence level is approximately 0.005. The turbulence level begins to increase at approximately 30° AOA. At 60° AOA, turbulence is up to 0.022. At Mach 0.4, the turbulence level at –10° AOA increases almost to the level at 40° AOA.[3]

Peak Dynamic Circumferential Distortion

Figure 6(a) shows the affect of AOA and AOSS on the peak dynamic circumferential distortion. Detrimental affects of AOA and AOSS on circumferential distortion are similar to those for inlet recovery. Comparing figure 6(a) with figure 5(a) shows that circumferential distortion increases as inlet recovery decreases, an anticipated result. The affect of AOSS is pronounced for all AOA at Mach 0.3. As the aircraft moves increasingly nose-left (positive AOSS), the peak dynamic distortion decreases. As the aircraft moves increasingly nose-right (negative AOSS), the peak dynamic distortion increases. From 4° to 30° AOA, the peak dynamic distortion increases slightly. Above 30° AOA, the peak dynamic distortion increases rapidly. This distortion approximately doubles from 0.08 at 30° AOA to 0.17 at 60° AOA.

Peak Dynamic Radial Distortion

Figure 6(b) shows AOA and AOSS having little affect on peak dynamic radial distortion up to 40° AOA. Increasing AOA from 40° to 60° causes the peak radial distortion to increase rapidly. Increasing AOA to 50° and 60° increases the sensitivity to AOSS, similar to the AOSS affect on circumferential distortion. Reference 3 provides additional details.

Inlet Distortion for Rapid AOA Maneuvers

To determine whether the results obtained during steady aerodynamic conditions were adequate for describing the inlet-generated, total-pressure distortion levels which occur during rapid AOA maneuvers, a series of positive and negative AOA sweeps were performed. Maximum rates of 46 deg/sec and –37 deg/sec were attained. Inlet recovery and peak distortion values were then compared with an estimated value based on equivalent steady aerodynamic conditions.

Figure 7 shows inlet recovery and circumferential distortion levels during a low- to high-AOA sweep at Mach 0.3 with AOSS near 0° compared with the steady aerodynamic estimation. Figure 7(a) shows the AOA sweep from 10° to 62° with corresponding AOSS. Figure 7(b) shows good agreement between the

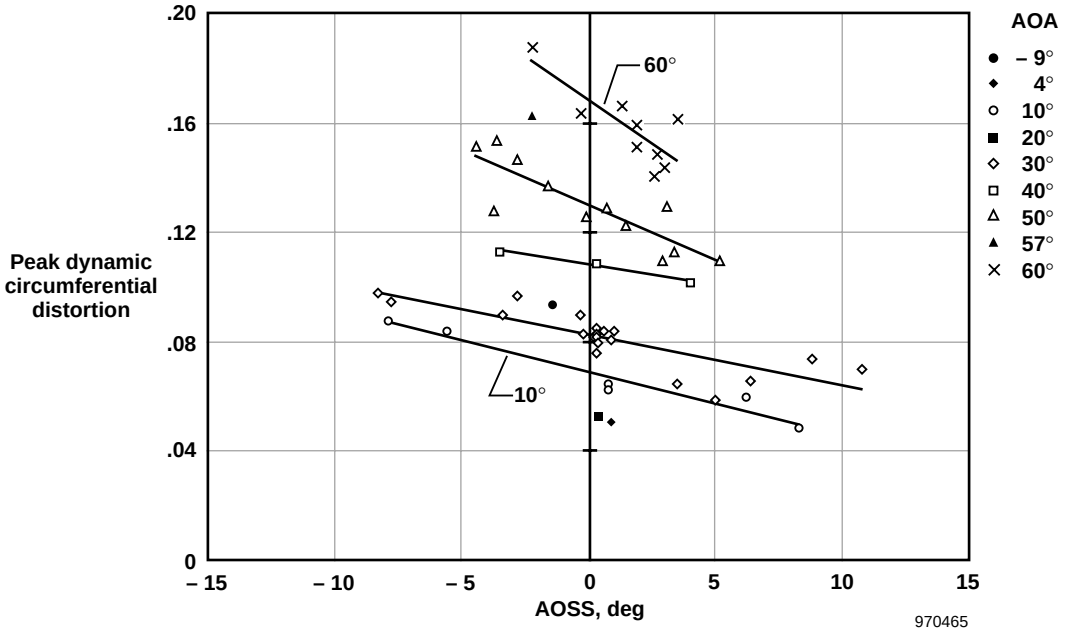

(a) Maximum peak dynamic circumferential distortion.

Figure 6. Affect of AOA and AOSS on peak dynamic circumferential and radial distortion during steady aerodynamic conditions at Mach 0.3.

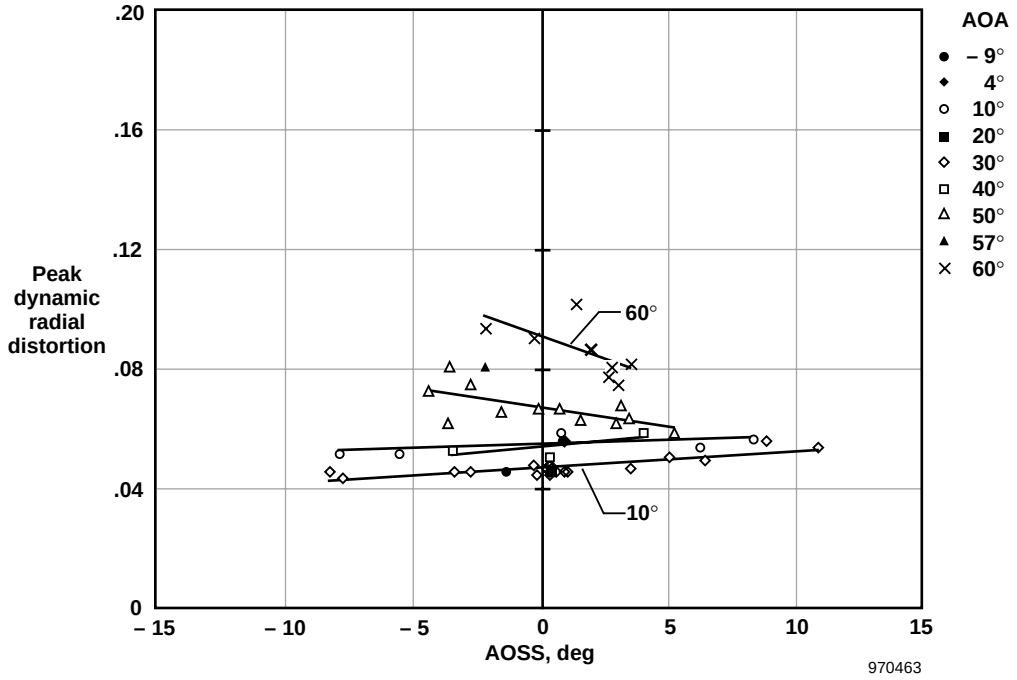

(b) Maximum peak dynamic radial distortion.

Figure 6. Concluded.

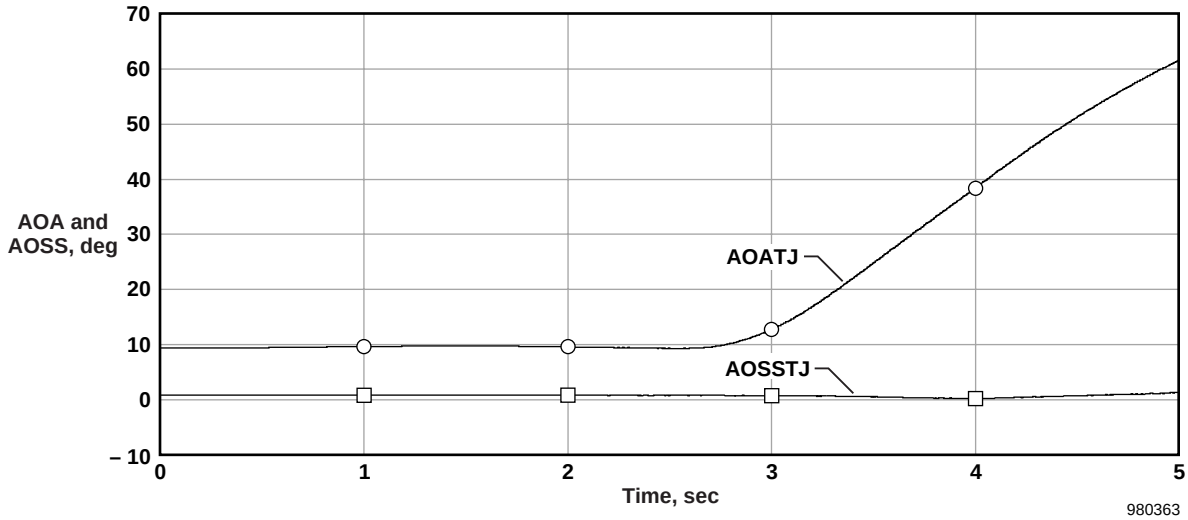

(a) AOA and AOSS, deg.

Figure 7. Time histories of inlet recovery and circumferential distortion compared with the steady estimation model during a low- to high-AOA sweep at Mach 0.3.

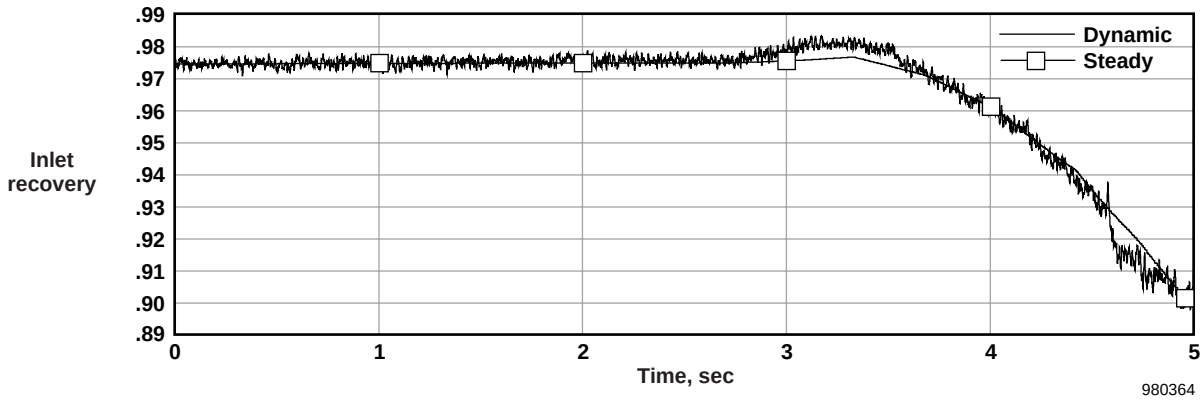

(b) Inlet recovery comparison.

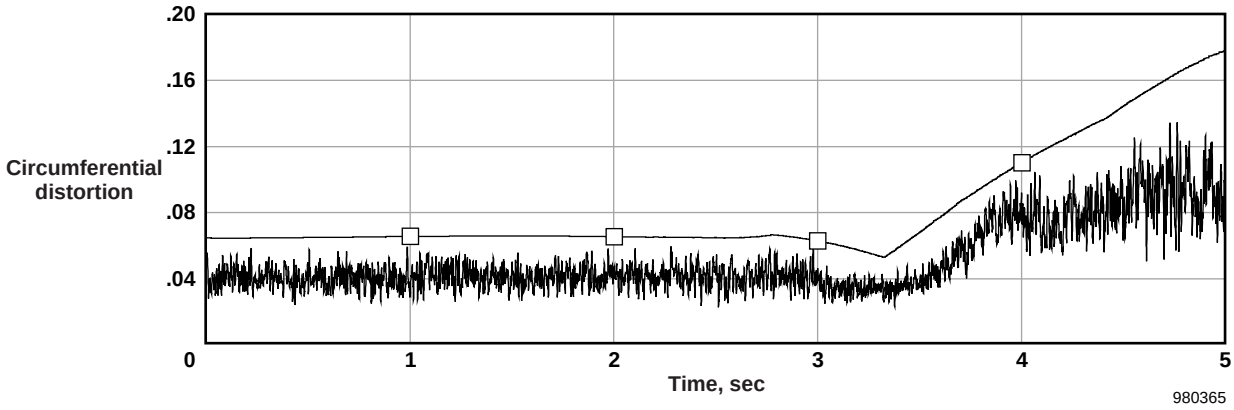

(c) Circumferential distortion comparison.

Figure 7. Concluded.

recovery level for the rapid AOA maneuver and the steady estimation model. A discontinuity in recovery at approximately 55° occurred. This discontinuity is believed to result from increased inlet flow separation. Figure 7(c) shows a comparison of the circumferential distortion levels. As expected, the level of distortion increases as high AOA is reached. The peaks in the circumferential distortion levels for the transient portions of the rapid AOA maneuver are less than the levels of the steady aerodynamic estimation model, which represents the maximum peaks at equivalent AOA. Reduced distortion levels were obtained for all AOA transients between 30° and 62°. The low distortion levels during rapid AOA transients confirm the current practice of fixed-attitude testing for obtaining peak distortion values. However, flight conditions were encountered where unexpected inlet recovery variations were obtained.

Figure 8 shows inlet recovery and circumferential distortion levels during a mid- to low-AOA sweep at Mach 0.3 compared with levels obtained from the steady aerodynamic estimation model of the maximum distortion levels. Figure 8(a) shows the AOA sweep from 28° to 0° and AOSS from –6° to 6°. Figure 8(b) shows good comparison for inlet recovery between the AOA sweep and the steady estimation model. Figure 8(c) shows a comparison of the circumferential distortion levels. Except between 0° and 2° AOA, the peaks in the circumferential distortion levels for this AOA maneuver were less than the levels obtained from the steady aerodynamic estimation model.

An examination of the other rapid AOA maneuvers verified that at a given flight condition, inlet distortion levels are less than the levels at an equivalent steady aerodynamic condition. The sudden change in the

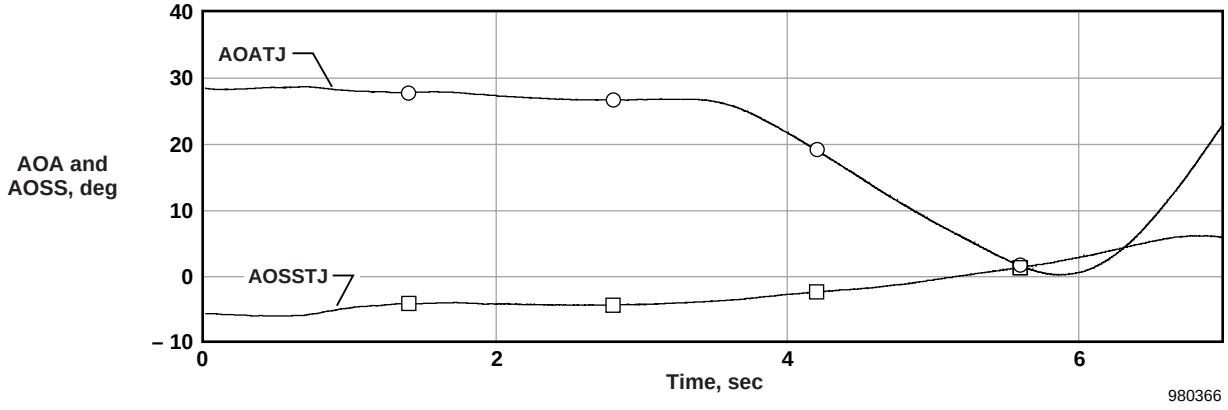

(a) AOA and AOSS, deg.

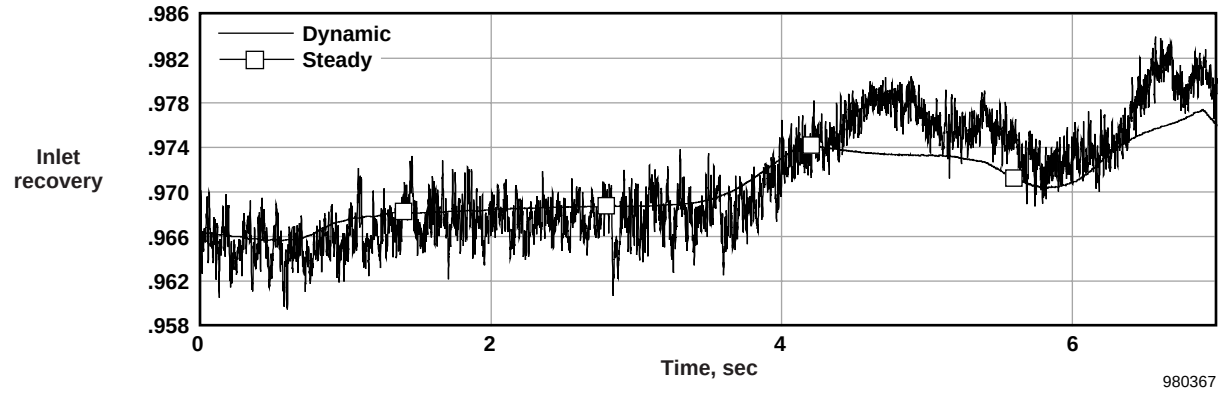

(b) Inlet recovery comparison.

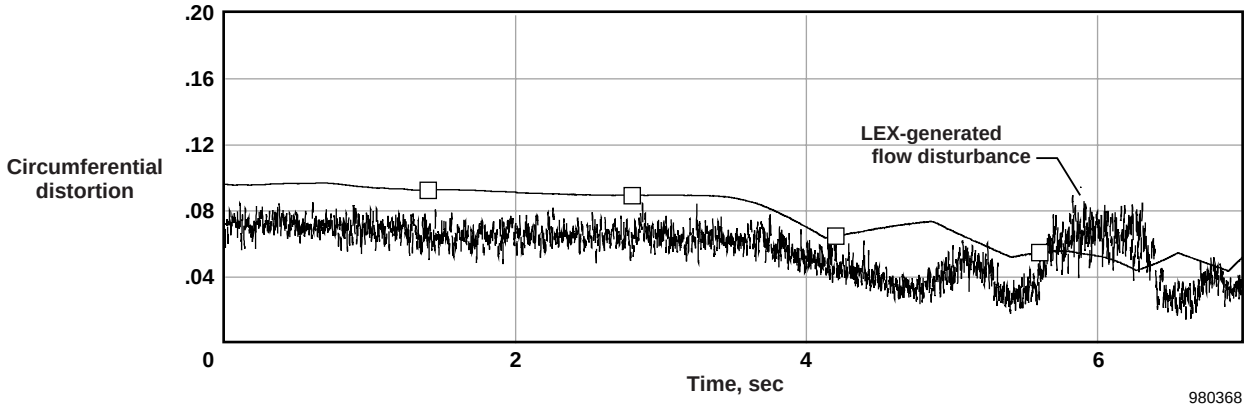

(c) Circumferential distortion comparison.

Figure 8. Time histories of inlet recovery and circumferential distortion compared with the steady estimation model during a mid- to low-AOA sweep at Mach 0.3.

distortion level near 0° AOA and as the aircraft moved from nose-right to nose-left is believed to result from an LEX-generated flow disturbance. Note also that the inlet recovery drops slightly near 0° AOA. The discrete steady aerodynamic conditions test matrix clearly did not provide a sufficiently detailed description of the inlet behavior during this maneuver. No steady aerodynamic data were obtained at 0° AOA. This result was observed in a number of low-AOA sweeps at Mach 0.3 and Mach 0.4. The maximum difference in recovery seen for the entire database was 0.005.

Inlet Distortion During Aircraft Departures

Twelve aircraft departures were achieved between Mach 0.3 and Mach 0.4 at 35 kft by pulling AOA to approximately 60° and inducing left or right yaw rates of 40 to 91 deg/sec. Engine stalls were obtained during 4 of the 12 departures. Figures 9–13 show data from a right-hand departure performed to a maximum yaw rate of 91 deg/sec. This departure induced two right-hand engine stalls. These stalls occur at approximately 10.8 and 14.6 sec and are indicated on these figures by event markers.

Figure 9 shows time histories of the aircraft aerodynamic positions (AOA and AOSS) and motions during a departure. The AOA and AOSS were obtained from a NASA trajectory reconstruction analysis procedure to correct for winds aloft. Figure 9(a) shows that AOA ranged from approximately 20° to 90°, and AOSS ranged from approximately –30° to 15°. Figure 9(b) shows the aircraft motion as described by rate of change of pitch, roll, and heading. These data were obtained from the INS and onboard rate gyroscopic measurements. For this departure, aircraft rates ranged from approximately –30 to 45 deg/sec for pitch rate, –5 to 70 deg/sec for roll rate, and 0 to 90 deg/sec for yaw rate.

Examining the pressure waveforms obtained from high-response instrumentation at the fan discharge and compressor discharge permits identification of the stall-initiating engine component. Figure 10 shows time histories of the discharge pressures and the engine inlet total pressure. The relative phasing and the direction of the pressure pertubations gives the sequence and propagation of the instability. An increase in pressure from the prestall level indicates that the pressure wave associated with stall initiation is propagating forward from high pressure located downstream of the measurement location. Analysis of the stall events which occurred during departed flight revealed that these stalls were initiated in the compressor. This result was unexpected because, based on F404-GE-400 distortion methodology, engine stalls caused by inlet maneuver distortion affects should be initiated in the fan. All of these engine stalls recovered without pilot action.

Figure 11 shows time histories indicating the variations of the inlet recovery and distortion parameters. Predicted loss of stability pressure ratios (DPRS) is also shown. The top of figure 11(a) shows

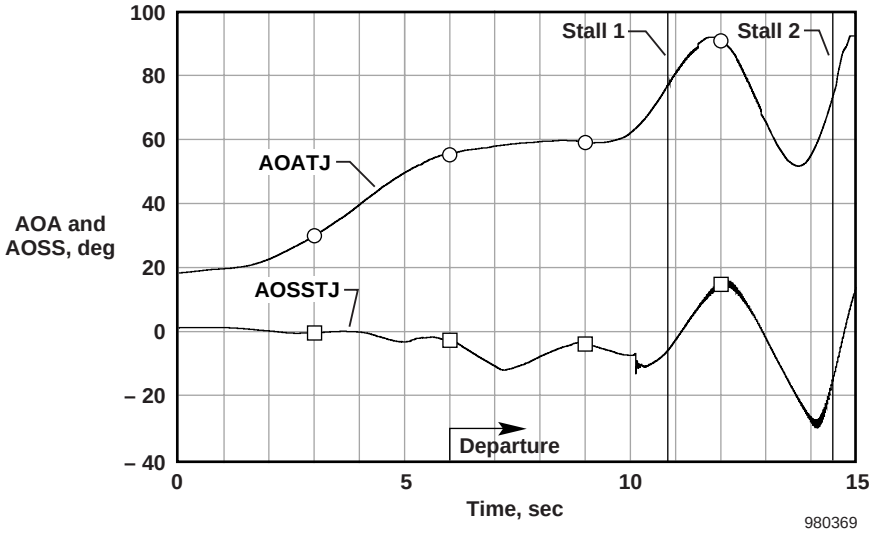

(a) AOA and AOSS, deg.

Figure 9. Time histories of aircraft aerodynamic positions and rates during a departure.

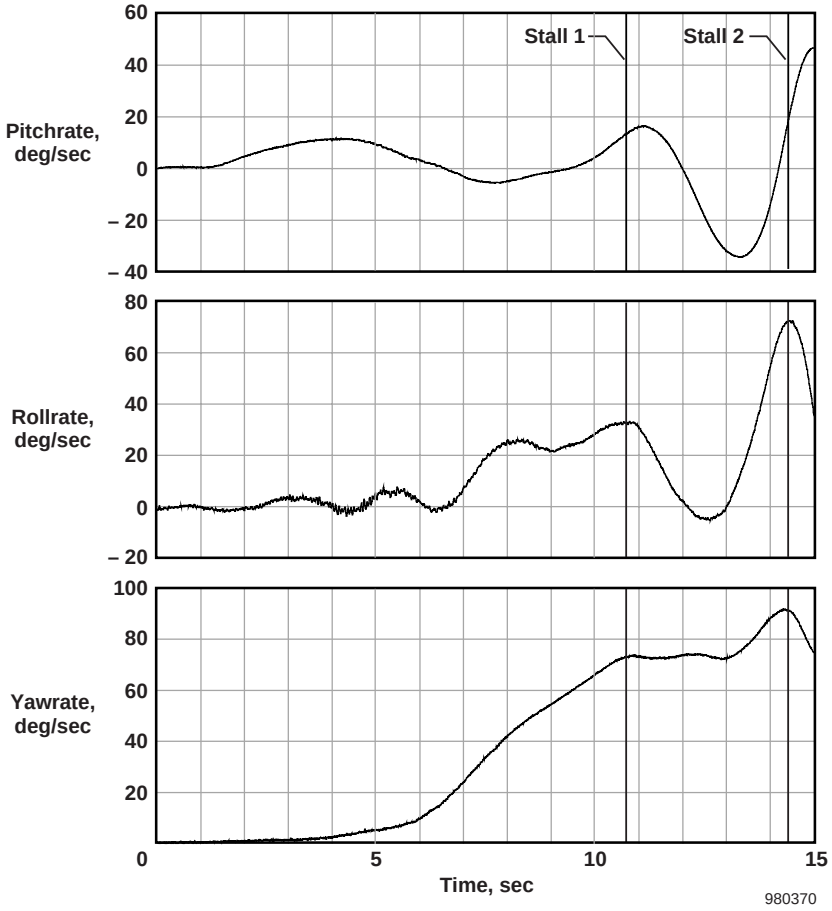

(b) Aircraft rates, deg/sec.

Figure 9. Concluded.

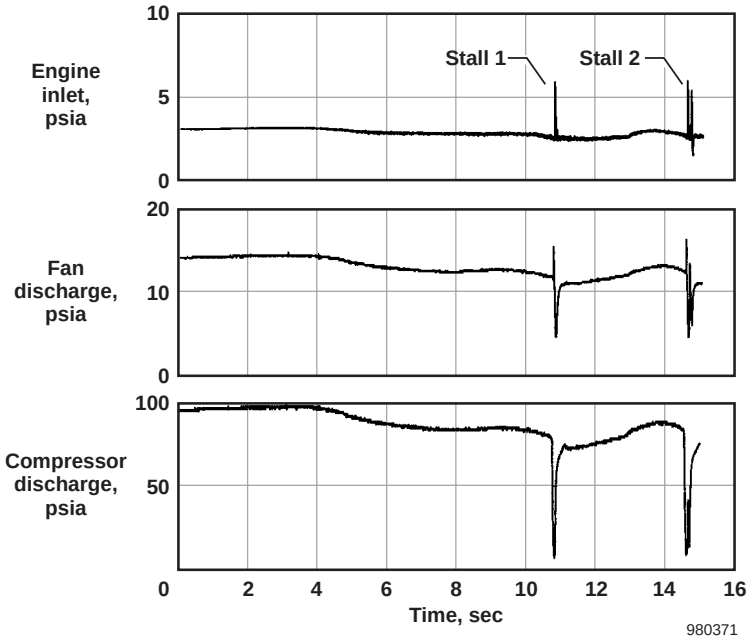

Figure 10. Time histories of measured inlet–engine entry and engine internal pressures.

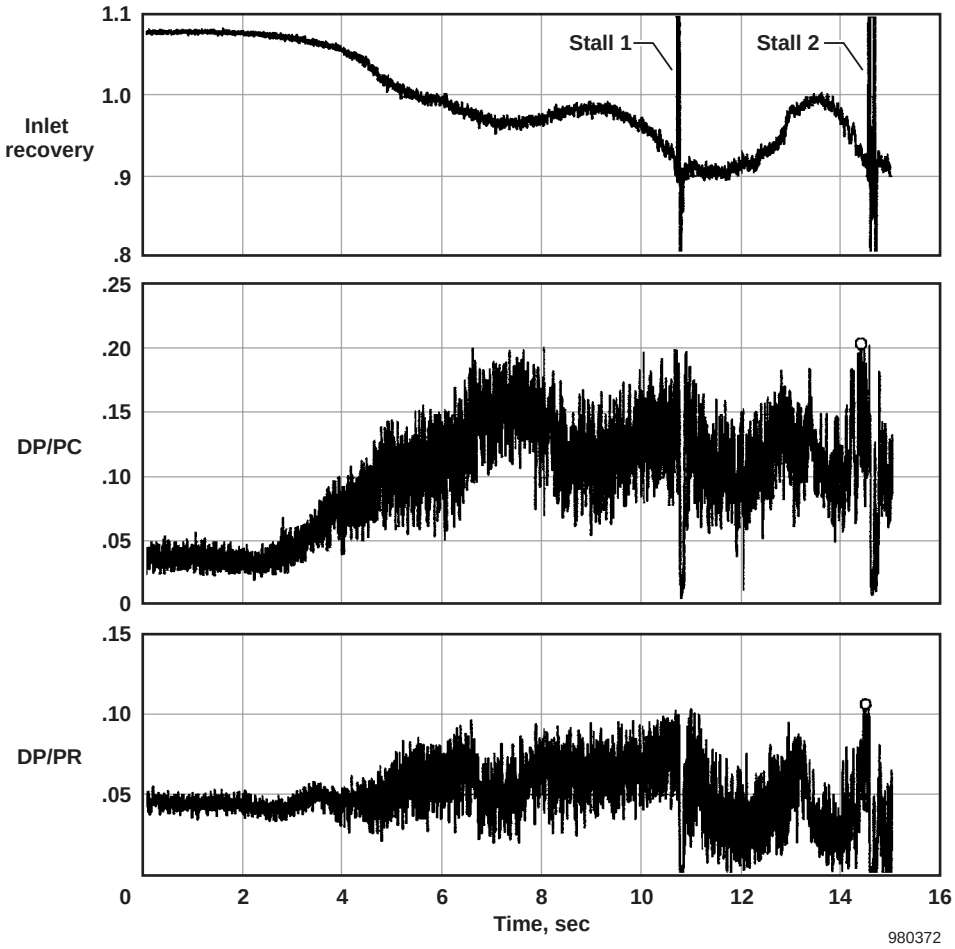

(a) Inlet recovery and distortion descriptors.

Figure 11. Time histories of inlet recovery, distortion descriptors, and predicted loss of stability pressure ratio for the fan and the compressor.

that the increase in AOA coupled with the decrease in AOSS caused a reduction in recovery and an increase in large, dynamic variations in the distortion descriptors. An examination of the departed flight maneuvers revealed that the magnitude of the peak time-variant, total-pressure distortion levels were well beyond those encountered in the normal engine operating envelope. The peak time-variant circumferential total-pressure distortion levels exceeded the limits used as guidance for the F404-GE-400 engine installation by as much as 25 percent.

Figure 11(b) shows the predicted losses of stability pressure ratio of the fan and the compressor resulting from the measured levels of time-varying spatial inlet total-pressure distortion. High levels of DPRS for the compressor (DPRSH) occur immediately before the stalls. However, there were many instances where equally high DPRSH levels occurred which did not initiate a stall. The occurrence of the stall events did not correlate with the magnitude of the distortion or the DPRSH levels alone. Other factors were involved.

Reviewing the stall data revealed that a parameter describing the combined rate of change of aircraft pitch, roll, and yaw would be an improved correlating factor of the stall events. Rates of change of aircraft motion produce gyroscopic moments. These moments and forces change the clearances of the rotor airfoils and thereby affect the stability limits of the compression components. For these reasons, a combined rate of change of aircraft motion parameter (CROCP) was defined by taking the root-sum-square of the pitch, roll, and yaw rates.

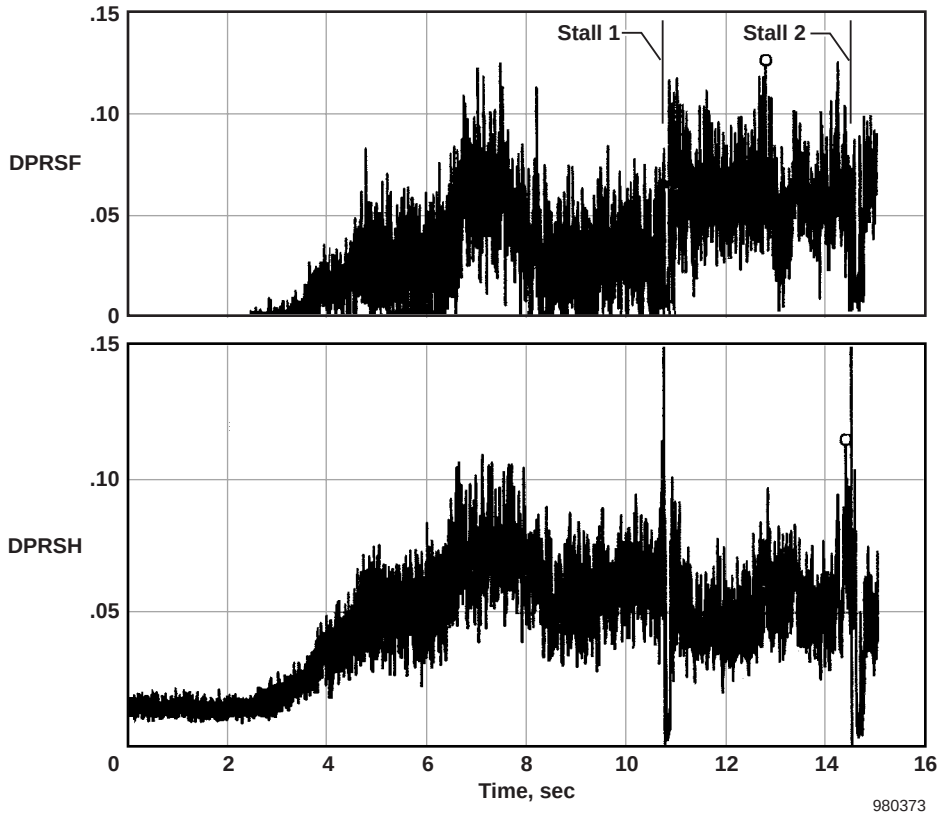

(b) Predicted loss of stability pressure ratio for the fan and compressor.

Figure 11. Concluded.

Figure 12 shows the stalls superimposed on the time history of the combined rate of change of aircraft motion. The stalls occur at local maximum values. Other departure-induced stalls exhibited the same behavior. However, maximum values of combined rate of aircraft motion alone were not an indicator of a stall.

By combining the affects of inlet distortion and aircraft motion, figure 13 shows the loss of compressor stability ratio as a function of the combined rate of change values throughout all of the departures at stall and at poststall. These stall data fall into two classes: isolated and non-isolated. The isolated data are characterized by no stall occurring during the previous 2.4 sec or more. The non-isolated stalls may have occurred because the engine did not have time to re-establish the thermal equilibrium characteristics that are associated with normal operation.

Of the 14 right-hand engine stalls, 7 were isolated stalls and 5 were non-isolated stalls. Data were not available for the two remaining stalls. These isolated stall data all tend to group at simultaneous high values of predicted DPRSH and CROCP as expected; meanwhile, the non-isolated stalls occurred at low combined values. Therefore, the isolated stalls which occurred during departed flight appear attributable to the combined affect of inlet total-pressure distortion on the compressor and compressor clearance changes. Changes in compressor clearance may result from eccentricity of the compressor rotor, distortion of the compressor casing caused by high rates of aircraft motion, or both.

CFD Inlet Distortion Prediction Comparison with Flight Data

A procedure was developed to estimate inlet dynamic distortion using CFD-computed data. Figure 14 shows that the prediction of the average total-pressure recovery at the AIP at low AOA were within 1 percent of the flight data. This result was typical for eight simulated flight conditions. At high AOA, the predicted recovery patterns

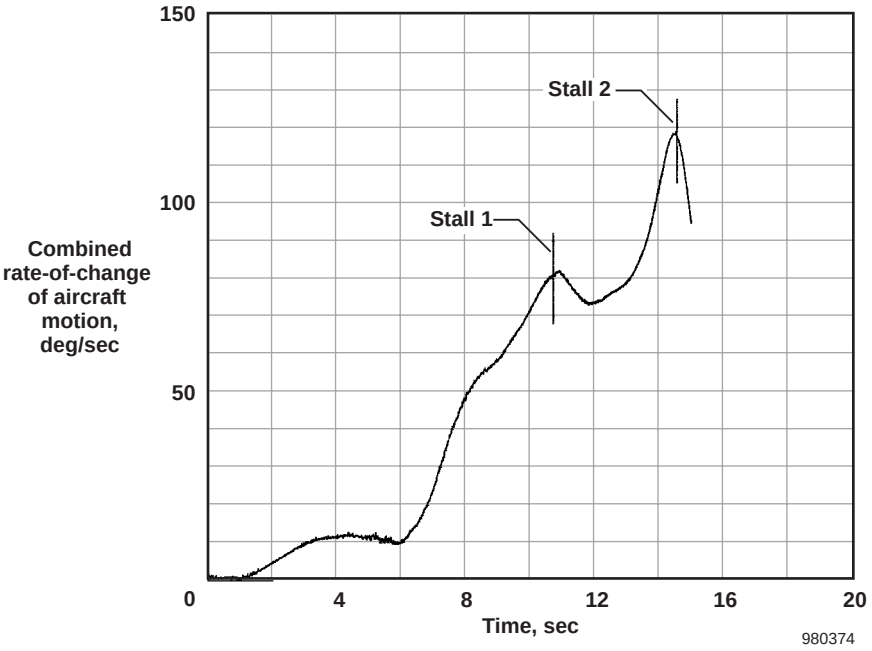

Figure 12. Time history of the combined rate of change of aircraft motion.

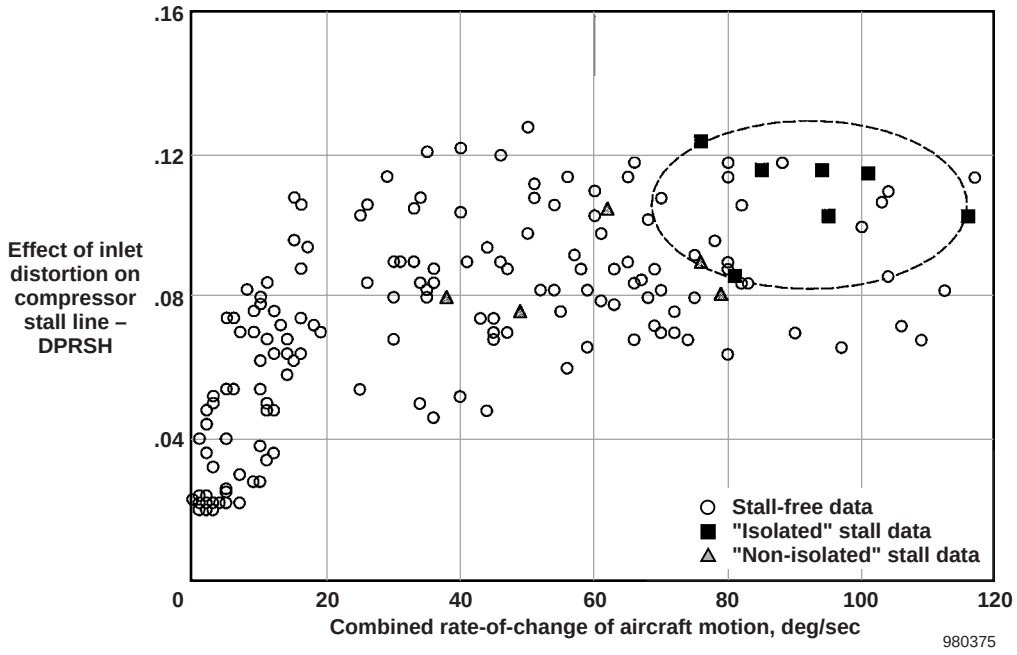

Figure 13. Affects of aircraft motion on time-variant inlet distortion on compressor stall line.

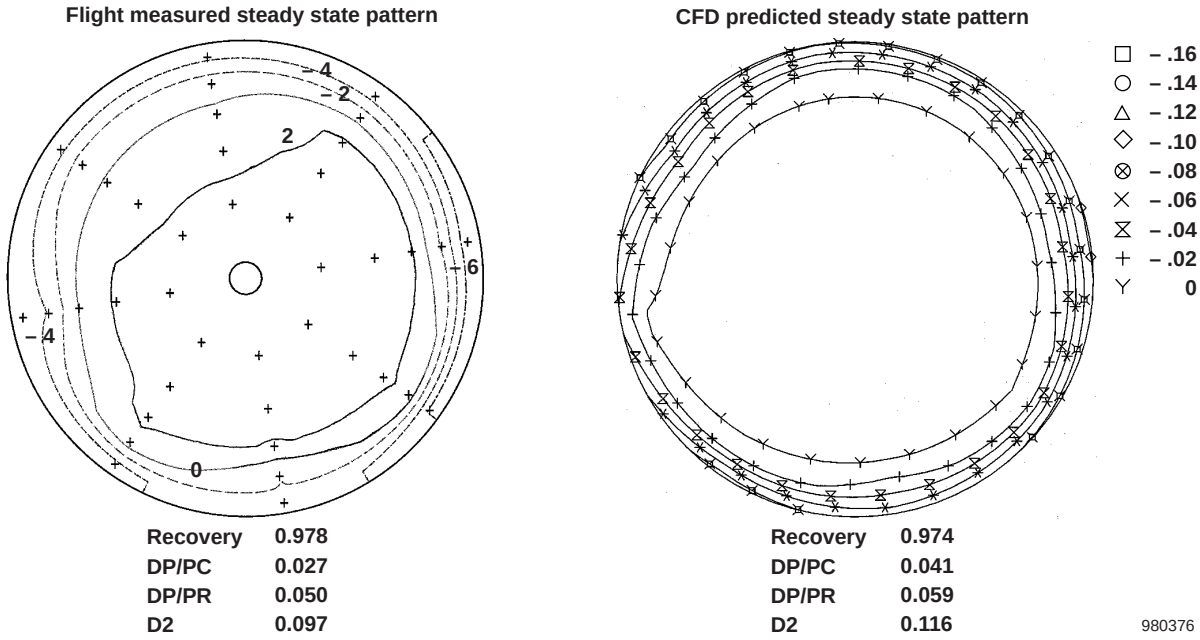

Figure 14. Steady-state total-pressure recovery comparisons at 3.6° AOA, Mach 0.4, and ALF.

were significantly different (fig. 15). The CFD-predicted minimum total pressures at the AIP were consistently less than the flight test data, which caused the predictions of dynamic distortion to be high in all cases.

Several suspected causes for the differences between predicted and measured engine face recovery patterns exist. An accurate computation of the vortices generated from the vortex generators is essential in computing accurate recovery patterns, in computing turbulence levels, and in synthesizing dynamic distortion. Small errors in the trajectories of these vortices can cause a large error in the interpolated value of a total pressure and erroneously dominate the synthesized patterns. The trajectory error is thought to be a strong function of the turbulence model. Another possible cause is modeling the engine effect. A simulation of a porous screen representing the engine face helped the predictions. Another cause for the CFD model deficiency is that mass flow is currently corrected using full CFD exit recovery, not a 40-probe average at the AIP. This difference in recovery can be as large as 0.8 percent. In addition, the inlet flow is assumed to be completely turbulent. An inlet boundary-layer transition region may exist which significantly affects the subsequent boundary-layer separation and vortex formation.

Engine Airflow Estimation

Impact of inlet-generated, total-pressure distortion on estimated levels of engine airflow was studied. Four airflow estimation methods were used. The reference method was a fan-corrected airflow to fan-corrected speed calibration from an uninstalled engine test. In-flight airflow estimation methods used the average, or individual, inlet duct static- to total-pressure ratios and the average fan-discharge static pressure to average inlet total-pressure ratio. Correlations were established at low distortion conditions for each method relative to the reference method. A range of distorted inlet flow conditions was obtained from –10° to 60° AOA and –7° to 11° AOSS.

Figure 16 shows a comparison of two of the four airflow estimation methods as a function of the reference method. The solid symbols represent data points where steady-state AIP total pressure patterns were generated and compared (fig. 30, ref 7). Figure 16(a) shows that the individual inlet probe pressure ratio method correlation resulted in a ±1.15-percent airflow spread for all distorted flow levels with a bias error of –0.7 percent. Figure 16(b) shows that the fan-discharge pressure-ratio method correlation resulted in a ±0.3-percent airflow spread with essentially no bias error. Inlet-generated total-pressure distortion and turbulence had no significant impact on engine airflow. As a result, a speed-flow relationship may provide the optimum airflow estimate for a specific engine under all flight conditions.

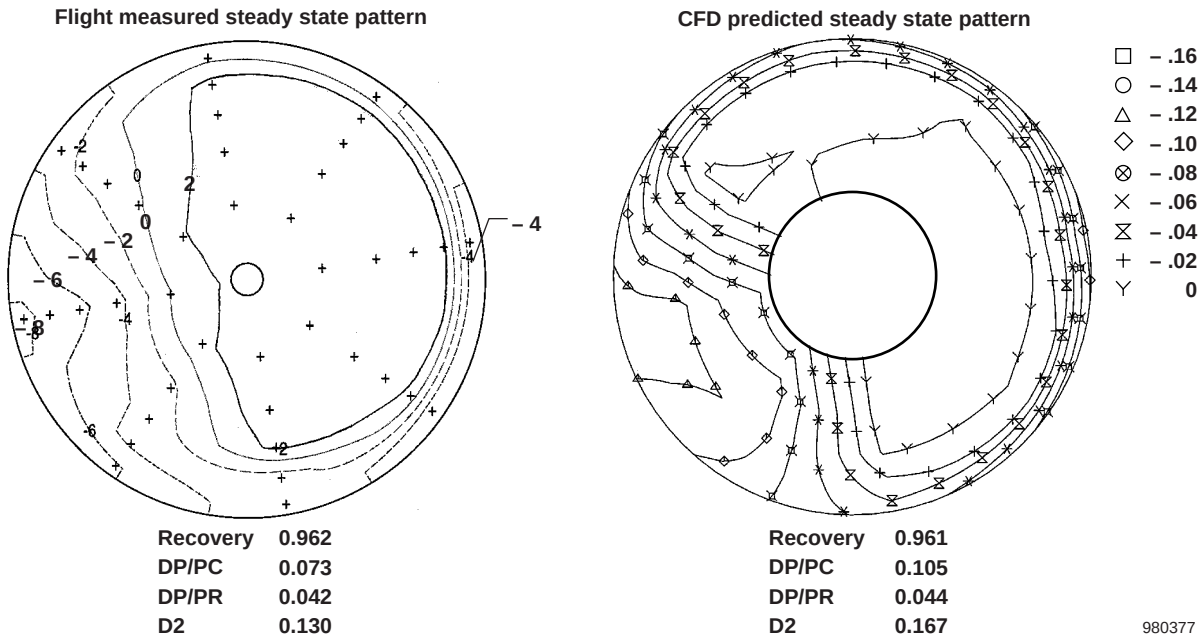

Figure 15. Steady-state total-pressure recovery comparisons at 39° AOA, Mach 0.4, and ALF.

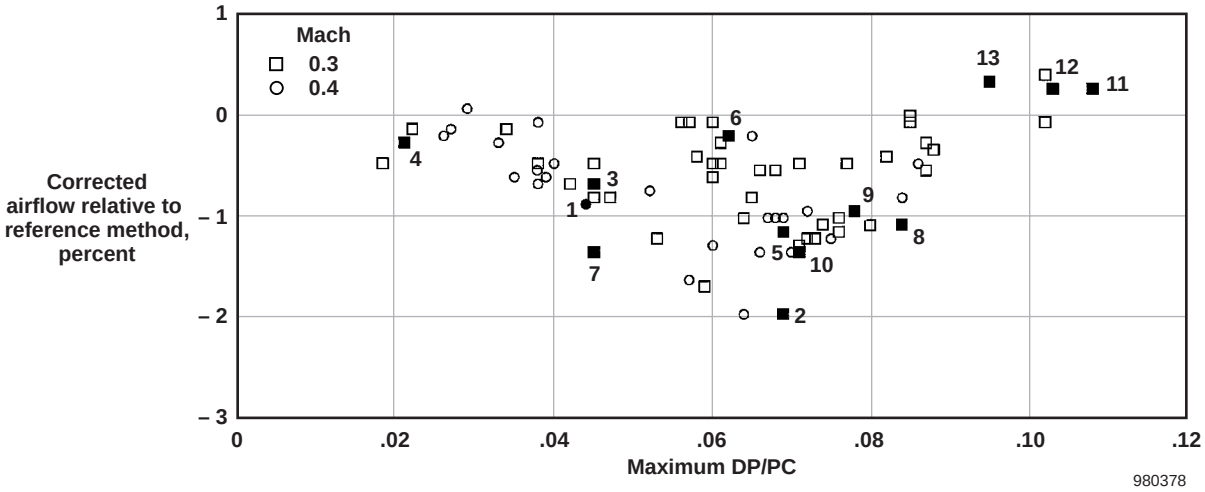

(a) Method 1.

Figure 16. Corrected airflow relative to reference method as a function of circumferential distortion level (adapted from ref. 7).

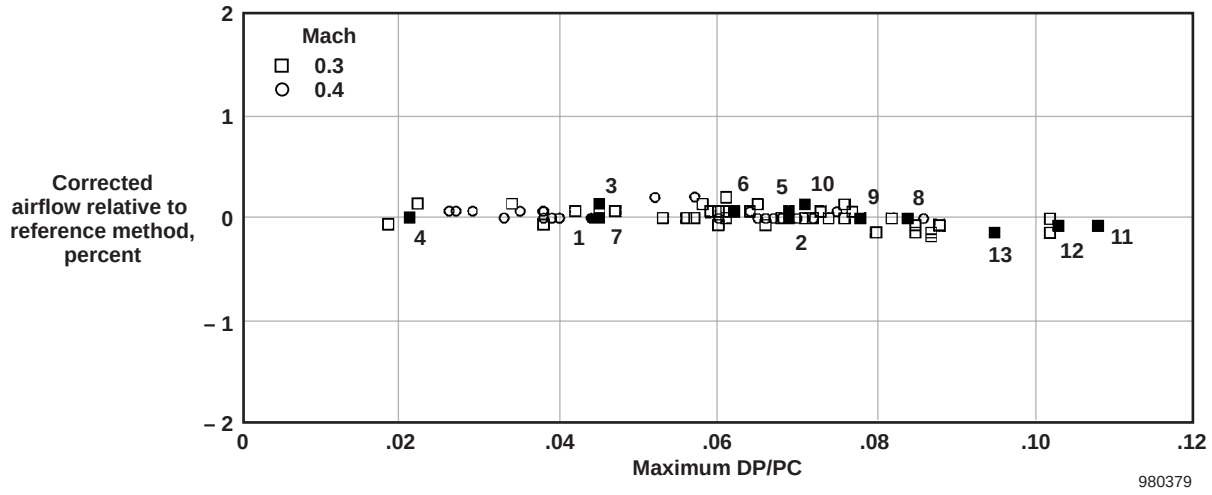

(b) Method 2.

Figure 16. Concluded.

Conclusions

An extensive inlet aerodynamic database was obtained for the NASA F/A-18A High Alpha Research Vehicle (HARV). High quality HARV inlet data allowed significant insights and increases in the understanding of inlet performance at high AOA and during rapid aircraft maneuvers. Inlet data obtained at Mach 0.3, at an angle of attack (AOA) of 30°, and at an angle of sideslip (AOSS) of 0° showed excellent repeatability. During steady aerodynamic conditions, inlet recovery and peak circumferential distortion increased as AOA increased and as AOSS became increasingly negative (nose-right). During rapid AOA maneuvers, it was verified that at a given flight condition, the maximum inlet distortion levels are less than at an equivalent steady aerodynamic condition. However, rapid maneuvers did identify aerodynamic conditions when discrete changes in inlet behavior occurred.

Twelve intentional aircraft departures were conducted to obtain inlet data leading to and during engine stalls. Results revealed that the magnitudes of the peak time-variant total-pressure distortion levels were well beyond those encountered in the normal engine-operating envelope. An unexpected result was that all engine stalls were initiated in the compressor, not in the fan as predicted.

The computational fluid dynamics predicted inlet distortion comparison with flight data shows that the prediction of the average total-pressure recovery at the low-AOA conditions evaluated was within 1 percent of the flight test data. At high AOA, the predicted recovery patterns were significantly different. Based on the study of four airflow estimation methods, the speed-flow relationship provides the best airflow estimate for a specific engine under all flight conditions.

References

[1]Regenie, Victoria, Donald Gatlin, Robert Kempel, and Neil Matheny, *The F-18 High Alpha Research Vehicle: A High-Angle-of-Attack Testbed Aircraft*, NASA TM-104253, 1992.

[2]Yuhas, Andrew J., Ronald J. Ray, Richard R. Burley, William G. Steenken, Leon Lechtenberg, and Don Thornton, *Design and Development of an F/A-18 Inlet Distortion Rake: A Cost and Time Saving Solution*, NASA TM-4722, 1995.

[3]Walsh, Kevin R., Andrew J. Yuhas, John G. Williams, and William G. Steenken, *Inlet Distortion for an F/A-18A Aircraft During Steady Aerodynamic Conditions up to 60° Angle of Attack*, NASA TM-104329, 1997.

[4]Yuhas, Andrew J., William G. Steenken, and John G. Williams, *F/A-18A Inlet Flow Characteristics During Maneuvers with Rapidly Changing Angle of Attack*, NASA TM-104327, 1997.

[5]Steenken, William G., John G. Williams, and Andrew J. Yuhas, *An Inlet Distortion Assessment During Aircraft Departures at High Angle of Attack for an F/A-18A Aircraft*, NASA TM-104328, 1997.

[6]Norby, W. P. and J. A. Ladd, A. J. Yuhas, *Dynamic Inlet Distortion Prediction with a Combined Computational Fluid Dynamics and Distortion Synthesis Approach*, NASA CR-198053, 1996.

[7]Williams, J. G., W. G. Steenken, and A. J. Yuhas, *Estimating Engine Airflow in Gas-Turbine Powered Aircraft with Clean and Distorted Flows*, NASA CR-198052, 1996.

[8]Sedlock, D., "Improved Statistical Analysis Method for Prediction of Maximum Inlet Distortion," AIAA-84-1274, June 1984.

[9]Amin, N. F., C. J. Richards, E. G. de la Vega, and M. A. Dhanidina, *F/A-18A Engine Inlet Survey Report*, vol. 1 of 3, NOR 81-316, Northrop Corporation, Aircraft Division, Hawthorne, California, Northrop FSCM 76823, November 1981.

[10]Morse, D. B., N. F Amin, F. W. Marxen, J. A. McGuire, E. G. de la Vega, and M. Yamadar, *Propulsion System Functional and Performance Analysis Report*, NOR 77-364, Northrop Corporation, Aircraft Division, Hawthorne, California, July 1978.

[11]Amin, N. F. and D. J. Hollweger, "F/A-18A Inlet/Engine Compatibility Flight Test Results," AIAA-81-1393, July 1981.

[12]Moes, Timothy R. and Stephen A. Whitmore, *A Preliminary Look at Techniques Used to Obtain Airdata From Flight at High Angles of Attack*, NASA TM-101729, 1990.

[13]Ray, R. J., J. W. Hicks, and R. I. Alexander, *Development of a Real-Time Aeroperformance Analysis Technique for the X-29A Advanced Technology Demonstrator*, NASA TM-100432, 1988.

[14]Thornton, D. A. and W. G. Steenken, *Summary of Inlet Distortion Rake Activities Flight Clearance Through High-Temperature Rake Delivery*, General Electric Aircraft Engines, Cincinnati, Ohio, October 1995.

[15]Society of Automotive Engineers, Inc., *Gas Turbine Engine Inlet Flow Distortion Guidelines*, Aerospace Recommended Practice 1420, Warrendale, Pennsylvania, March 1978.

[16]Society of Automotive Engineers. Inc., *Inlet Total-Pressure-Distortion Considerations for Gas-Turbine Engines*, Aerospace Information Report 1419, Warrendale, Pennsylvania, May 1983.

[17]P. M. Shumate, *GE Distortion Analysis Program Users' Manual*, version 3, GEAE TM-88-352, General Electric Aircraft Engines, Cincinnati, Ohio, September 1988.

[18]General Electric Aircraft Engines, *Model Specification for F404-GE-400 Turbofan Engine*, Specification no. CP45K0006, Cincinnati, Ohio, November 1975, Reprinted February 1983.